Biosensors and Bioelectronics 218 (2022) 114742

Contents lists available at ScienceDirect

Biosensors and Bioelectronics

journal homepage: www.elsevier.com/locate/bios

# A green route for lignin-derived graphene electrodes: A disposable platform for electrochemical biosensors

Lingyin Meng [a,**], Sorana Chirtes [a], Xianjie Liu [b], Mats Eriksson [a], Wing Cheung Mak [a,c,*]

[a] Division of Sensor and Actuator Systems, Department of Physics, Chemistry and Biology, Linköping University, SE-581 83, Linköping, Sweden
[b] Laboratory of Organic Electronics, Department of Science and Technology, Linköping University, SE, 60174, Norrköping, Sweden
[c] Department of Biomedical Engineering, The Chinese University of Hong Kong, Hong Kong SAR, China

ARTICLE INFO

*Keywords:*
Lignin
Laser lithography
Patterning
Reduced graphene
Disposable electrodes

ABSTRACT

The tremendous growth of disposable electrode-based portable devices for point-of-care testing requires mass production of disposable electrodes in a low-cost and sustainable manner. Here, we demonstrate a green route for the conversion of biomass lignin, patterning, and reduction of the lignin-derived graphene electrodes by sequential laser lithography, water lift-off and sodium borohydride ($NaBH_4$) treatment, and their use for electrochemical lactate biosensors. Energy-saving and localized laser lithography converted the aromatic ring-rich lignin into porous laser-induced graphene (LIG). The conductivity and attachment of the LIG to the substrate were optimized in a factorial experiment with laser power and scan speed as variables. Characterization results revealed the conversion of partial heteroatoms (e.g., Na, S, O) into granular inorganic compounds on the LIG surface under laser treatment. Water was used as an eco-friendly solvent for the patterning of the LIG (P-LIG) by a lift-off process, where the inorganic residues and un-reacted lignin were dissolved, exposing the macro-/micro-pores in the P-LIG. $NaBH_4$ induced a reduction of the P-LIG (P-rLIG) resulting in improved electrochemical kinetics with lower charge transfer resistance (27.3 Ω) compared to the LIG (248.1 Ω) and the P-LIG (61.4 Ω). The porous P-rLIG served as a 3D electrode for the deposition of Prussian blue and lactate oxidase for disposable electrochemical lactate biosensors, delivering a good analytical performance towards lactate detection with a linear range up to 16 mM and a high sensitivity (1.21 μA $mM^{-1}$). These lignin-derived disposable electrodes, utilizing renewable resources together with low-energy consumption fabrication and patterning, may contribute to the sustainable manufacturing of biosensors for point-of-care and point-of-use applications.

## 1. Introduction

Disposable electrodes have been widely used in electrochemical biosensors for point-of-care testing (POCT) of key biomarkers in biological samples, which provides efficient chronic disease monitoring and health care management in decentralized locations because of their high specificity and ease-of-operation (Ahmed et al., 2016; Newman and Turner, 2005). The conversion of biomarker levels into electrochemical signals relies on bioreceptor-immobilized and functional material-modified electrodes connected to a portable device (Turner, 2013). The disposable nature of these electrodes provides avoidance of electrode fouling induced loss of sensitivity, prevention of cross-contamination and cross-infection between different subjects as well as ease of modification (Bettazzi et al., 2017), in a similar manner as disposable ECG electrodes (Pani et al., 2018), glucose test strips (Newman and Turner, 2005) and screen-printed electrodes (Mohamed, 2016). This, in turn, requires mass production of disposable electrodes at low-cost and in high volumes. In addition, efforts have been devoted to the fabrication of patterned, flexible, and skin-mountable electrodes for wearable sensors and biosensors (Meng et al., 2020; Xu et al., 2019). What's more, green routes for material fabrication, via either eco-friendly and energy-saving techniques (Lee et al., 2017) or sustainable and non-toxic materials (Pradhan et al., 2020), are also needed to create a sustainable society in various applications, such as catalysis

* Corresponding author. Division of Sensor and Actuator Systems, Department of Physics, Chemistry and Biology, Linköping University, SE-581 83, Linköping, Sweden.
** Corresponding author. Division of Sensor and Actuator Systems, Department of Physics, Chemistry and Biology, Linköping University, SE-581 83, Linköping, Sweden.
*E-mail addresses:* lingyin.meng@liu.se (L. Meng), wing.cheung.mak@cuhk.edu.hk (W.C. Mak).

https://doi.org/10.1016/j.bios.2022.114742
Received 18 July 2022; Received in revised form 7 September 2022; Accepted 16 September 2022
Available online 20 September 2022

(Mahdi et al., 2022), energy generation and storage (Ma et al., 2017; Yousefi et al., 2019), environmental treatment (Yousefi et al., 2021), sensors and biosensors (Yan et al., 2017; Zhao et al., 2021) etc.

Biomass-derived resources have been explored in the fabrication of disposable electrodes for electrochemical biosensors due to their natural abundance and environmentally benign features, mainly serving as inexpensive substrates (e.g., cellulose) (Moro et al., 2019; Yáñez-Sedeño et al., 2020). Beyond this, biomass-derived resources can be used as precursors for carbonaceous materials as the active component in disposable electrodes (Pistone and Espro, 2020). For instance, lignin, as a highly heterogeneous binder between cellulose and hemicellulose, is the second most abundant natural polymer accounting for 20–30% of the lignocellulosic biomass. Despite its low-cost and bio-renewable nature, the lignin extracted from lignocellulosic biomass is mainly discarded as waste in the paper industry, with only ~2% used as concrete additives, stabilizing agents or dispersants and surfactants (Zhu et al., 2020). Accordingly, it has been an interesting topic to broaden the spectrum of lignin utilization strategies from both the research and industrial community. Based on the cross-linked aromatic ring structure, lignin can be converted into carbonaceous materials by conventional carbonization processes via either pyrolysis under an inert gas atmosphere, hydrothermal reaction or ionothermal carbonization (Wang et al., 2017; Zhang et al., 2021). However, these carbonization techniques usually result in lignin char or amorphous carbon powders with high content of heteroatoms (Zhang et al., 2021), which cannot fulfil the requirement of high electrical conductivity for the active component in disposable electrodes, resulting in limited charge transfer and low sensitivity. Thus, a graphitization step using high temperature (usually >2000 °C) in an inert gas is needed for the enlargement of graphene nanodomains into graphene/graphite structures with high conductivity (Fang et al., 2017; Zhang et al., 2021), which, however, is energy-consumable and cost-inefficient. Moreover, further application of such graphene/graphite powders requires their dispersion in non-renewable, toxic organic solvents (e.g., N-methyl-2-pyrrolidone, dimethylformamide), as well as mask-patterning and deposition onto a substrate for energy storage and sensing applications (Htwe et al., 2021; Wang et al., 2017; Xiong et al., 2021). Therefore, it is interesting to explore a green route for the *in-situ* simultaneous conversion and patterning of carbonaceous material-based disposable electrodes.

Recently, laser irradiation technology has been used for the fabrication of patterned carbonaceous electrodes from carbon-rich precursors such as graphene oxide and polyimide (El-Kady and Kaner, 2013; El-Kady et al., 2012; Meng et al., 2021). When the laser beam is scanned over the precursor film, the irradiated precursors absorb excitation energy, causing either a photochemical reaction (UV laser) with the direct breaking of chemical bonds and removal of the oxygen residuals, or a photothermal reaction (IR laser) with local heating for the breaking of weak chemical bonds and re-organization of the aromatic rings (Li, 2020). In the meantime, the dissociated oxygen is usually evolved and released in gaseous products (e.g., CO, $CO_2$, $H_2O$), resulting in an interconnected 3 dimensional (3D) graphene film (Lin et al., 2014; Srinivasan et al., 1994). Furthermore, laser irradiation can realize contact-free and mask-free construction of carbon patterns by the scanning of the laser beam with a moving platform (x-/y-direction) according to computer-aided designs, i.e., laser lithography. Such laser lithography provides an eco-friendly and energy-saving technique via the lower power consumption (usually ~40 W for an IR laser) and the localization of the laser beam spot on the precursors compared to the high temperature furnace for pyrolysis (Fenzl et al., 2017; Meng et al., 2021). In this manner, the conversion of lignin into patterned graphene structures has been used for microsupercapacitors (Ye et al., 2017; Zhang et al., 2018) and printed electronics (Edberg et al., 2020).

Herein, we demonstrate a green route for the conversion of biomass lignin, patterning, and reduction of the lignin-derived graphene electrodes by sequential laser lithography, water lift-off and sodium borohydride ($NaBH_4$) treatment, which serve as a disposable electrode platform with improved kinetics for the development of electrochemical biosensors. As shown in Scheme 1, a processable lignin solution with poly(vinyl alcohol) (PVA) as a binder was blade-coated on a flexible polyethylene terephthalate (PET) substrate into a homogenous lignin-PVA film for laser treatment. The laser converts the lignin-PVA into laser induced graphene (LIG). The conductivity and the attachment of the LIG to the substrate were optimized in a factorial experiment. The conversion of lignin into graphene was characterized by different spectroscopy and microscopy methods, showing that the partial heteroatoms (e.g., Na, S, O) were converted into granular inorganic compounds on the LIG surface. Water was used as an eco-friendly solvent to enable patterning of the LIG (P-LIG) by a lift-off process, where inorganic residues and un-reacted lignin-PVA were dissolved, thereby exposing the macro-/micro-pores in the P-LIG. As a reductant, $NaBH_4$ contributes to the reduction of the P-LIG (P-rLIG) with increased conductivity and improved electrochemical kinetics. The P-rLIG was functionalized with "artificial" (Prussian blue, PB) and natural (lactate oxidase, LOx) enzymes into a disposable electrochemical lactate biosensing electrode, delivering a competitive analytical performance towards lactate detection, providing a flexible and skin-mountable electrode for the non-invasive monitoring of lactate in sweat.

## 2. Experimental section

### 2.1. Materials and instruments

The details are given in the Supporting Information.

### 2.2. Deposition of lignin on a PET substrate via blade-coating

The lignin-PVA film was coated on a flat PET substrate via blade-coating. Firstly, the PET sheet was ultrasonically cleaned using acetone and isopropanol for 5 min, respectively, followed by air plasma treatment for 5 min. The lignin-PVA solution was prepared by dissolving 10 g lignin powder into 100 mL PVA aqueous solution (10%) under magnetic stirring for 12 h, followed by 30 min of sonication for the removal of bubbles. Coating of the lignin-PVA on the PET substrate was conducted using a Coatmaster-510 XL film applicator (Erichsen, Germany) with a heated platform (50 °C), a 120 μm gap between the cylinder blade and substrate and a coating speed of 60 mm/s. The resulting sample was dried in air for 12 h and denoted as lignin-PVA/PET.

### 2.3. Preparation of the LIG via laser lithography

Laser lithography of the lignin-PVA/PET was performed with a computer-controlled HL40-5g Full Spectrum Laser platform (Full Spectrum Laser LLC, USA) with a $CO_2$ laser (10.6 μm) operating with a 1000 ppi resolution in a raster mode under ambient condition. The full laser scan speed is 80 inches $s^{-1}$ and the full power is 40 W. The laser lithography efficiency of lignin-PVA/PET and its conversion into LIG was evaluated at different laser scan speeds (5–100%) and varying laser powers (5–100%). A standalone working electrode (3 mm diameter) and a three-electrode system including a working electrode (WE), a reference electrode (RE), and a counter electrode (CE) with a sensing area, a track, and a contact pad were prepared using the optimized power and scan speed parameters. Details of the electrode pattern design are provided in Fig. S1.

### 2.4. Patterning and reduction of the LIG

After the laser lithography, the unexposed lignin-PVA was removed by a water lift-off procedure by immersing the film in water for 30 min (Fig. S1). The patterned LIG was denoted P-LIG. The P-LIG was further treated with $NaBH_4$ to increase the conductivity by immersing the electrodes in a $NaBH_4$ solution (50 mM in NaOH, pH 10) for 1 h, followed by rinsing in water 3 times. The reduced P-LIG was denoted P-

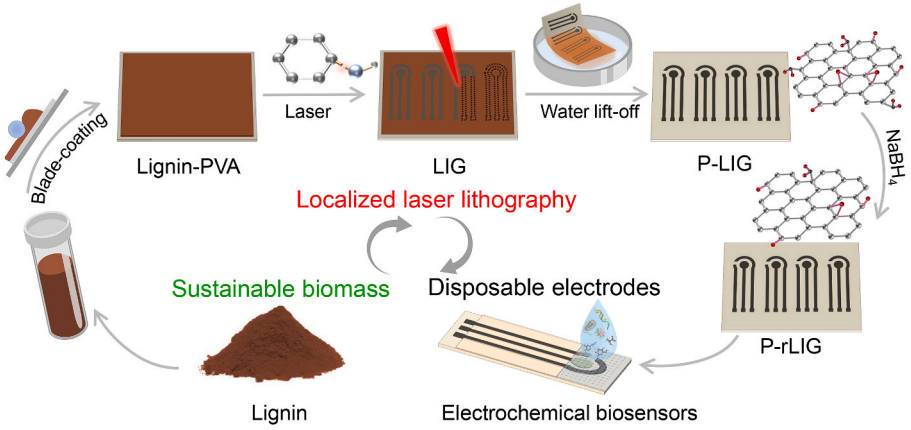


**Scheme 1.** A green route for the conversion of lignin, patterning and reduction of the lignin-derived graphene that enables disposable electrodes for electrochemical biosensors.

rLIG (Fig. S1). The conductive track of the electrode was isolated with Kapton tape to expose only the working electrode area and the contact pad for further experiment.

### 2.5. LIG functionalization for the electrochemical lactate biosensor

The three-electrode system was used for electrochemical lactate biosensors. No further treatment is needed for the counter electrode. The reference electrode was coated with Ag/AgCl ink using a paintbrush and a PET stencil for a confined coating zone, which was cured on a hotplate at 120 °C for 2 min. For the working electrode, Prussian blue (PB) was modified via potentiodynamic deposition over −0.4 to 0.7 V in 0.1 M KCl and HCl containing a 5 mM mixture of $K_3Fe(CN)_6$ and $FeCl_3$ for 10 cycles (scan rate 50 mV $s^{-1}$), followed by activation with cyclic voltammetry over −0.2 to 0.4 V in 0.1 M KCl and HCl for 10 cycles (scan rate 50 mV $s^{-1}$). The final electrode was rinsed with water, dried in air, and was denoted PB/P-rLIG. The PB/P-rLIG was immobilized with LOx for the fabrication of electrochemical lactate biosensors. In brief, an aliquot of enzyme suspension (3 μL) containing 40 mg $mL^{-1}$ LOx and 10 mg $mL^{-1}$ BSA was deposited on the PB/P-rLIG and dried at 4 °C for 2 h, followed by the addition of 2 μL chitosan solution (1%, in 1% acetic acid). The final enzyme electrode was denoted as LOx/PB/P-rLIG and stored at 4 °C when not in use. Finally, a porous polycarbonate membrane (0.2 μm) was placed over the 3-electrode area as an encapsulation layer.

### 2.6. Electrochemical measurements

Electrochemical measurement of the LIG, P-LIG and P-rLIG electrodes were performed with a CompactStat potentiostat (Ivium, Netherlands). Cyclic voltammetry (CV) and electrochemical impedance spectroscopy (EIS) of standalone working electrodes were conducted in 0.1 M KCl containing 5 mM $Fe(CN)_6^{3-/4-}$. For the integrated 3-electrode system of the electrochemical biosensor, all the electrochemical measurements were conducted with the internal Ag/AgCl as RE and the P-rLIG as CE. Amperometric hydrogen peroxide sensing and lactate biosensing using the integrated 3-electrode system was performed under a static mode in PBS and artificial sweat, respectively. The artificial sweat was prepared according to the European standard EN1811:2012 containing sodium chloride (0.5%), potassium chloride (0.1%) and urea (0.1%) and the pH was adjusted to 6.5 with ammonium hydroxide. Human sweat samples for real sample analysis were obtained from two healthy volunteers after running for 30 and 60 min, respectively. The sweat samples were collected from the forehead using sterile absorptive pads, followed by sweat extraction via centrifuge. The samples were analyzed by two LOx/PB/P-rLIG electrodes via amperometry at −0.15 V with a 3-fold dilution in artificial sweat. A standard colorimetric assay (lactate assay kit, Sigma-Aldrich) was conducted as a reference.

## 3. Results and discussion

### 3.1. Factorial optimization of the laser lithography

The laser power and scan speed are critical for the graphitization yield of lignin and the retention of the resulting LIG on the PET substrate without additional adhesives. As shown in Fig. 1, the laser power (*x*-axis) varied from 5% to 100% of the full power (40 W) with the scan speed (*y*-axis) increasing from 5% to 100% of the full scan speed (80 inches $s^{-1}$). The total energy per surface area delivered is lowest in the lower left corner and highest in the upper right corner of Fig. 1. Sheet resistances (S.R.) of the resulting LIG were measured to evaluate the synergistic effect of laser power and laser scan speed on the graphitization yield of lignin-PVA. Fig. 1 shows the common logarithm (base 10) of the S.R. values, which are color coded to visualize the results as a heat map. The corresponding images of lignin-PVA/PET showed a successful conversion of lignin into conductive graphene, with a characteristic black color under specific combinations of power and scan speed (Fig. S2). It is not effective (N.E.) for the conversion of lignin into graphene with a laser power lower than 20%. With increasing laser power in the medium range (20–60%), the resulting graphene on the PET surface appeared darker in color and the sheet resistance decreased gradually (Fig. 1). However, with the laser power higher than 60%, the laser etched through the PET substrate and caused an impaired film (I.F.) due to high laser intensity. On the other hand, high scan speed caused a high sheet resistance (H.S.R.), while lowering the scan speed facilitated the conversion of lignin into graphene via longer exposure time resulting in a decreased sheet resistance value. Therefore, the combinations of medium laser power (20–60%) and medium to low scan speed (5–60%), illustrated as the red color zone in Fig. 1, are favorable for the conversion of lignin into graphene films with low resistivity.

Next, the LIG was processed for further patterning via lift-off with water to remove the excess lignin-PVA that was not irradiated by the laser. We found that the lower scan speeds are advantageous for the retention of the patterned LIG on the PET substrate after water lift-off treatment, while the LIG obtained from high scan speeds tends to float off from the PET substrate (Fig. S3). This can probably be ascribed to the deeper penetration of the laser at low scan speed resulting in the melting of the upper thin PET layer for anchoring the graphene layer (Fig. S4). Considering all these results, we chose a power of 35% and a scan speed of 35% as the optimized parameters for the preparation of LIG electrodes hereafter. We further demonstrated that the lignin-derived LIG process is versatile to other flexible substrates including the thermoplastics

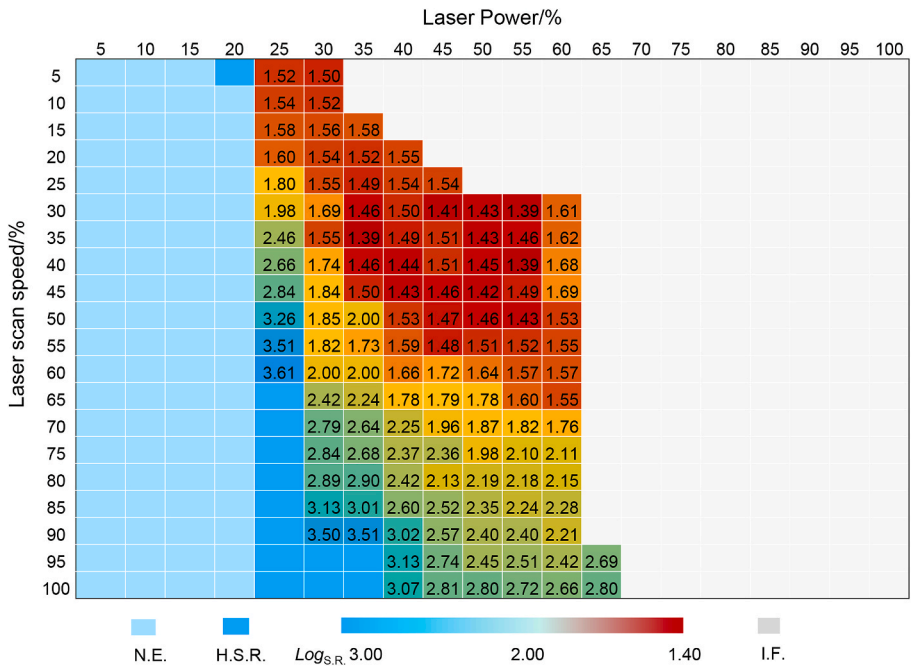


**Fig. 1.** Multifactorial optimization of laser lithography visualized as a heatmap. Color bar, N.E.: not effective; H.S.R.: high sheet resistance; LogS.R.: log10(x), x is the sheet resistance value in Ω/sq; I.F.: impaired film due to high laser intensity.

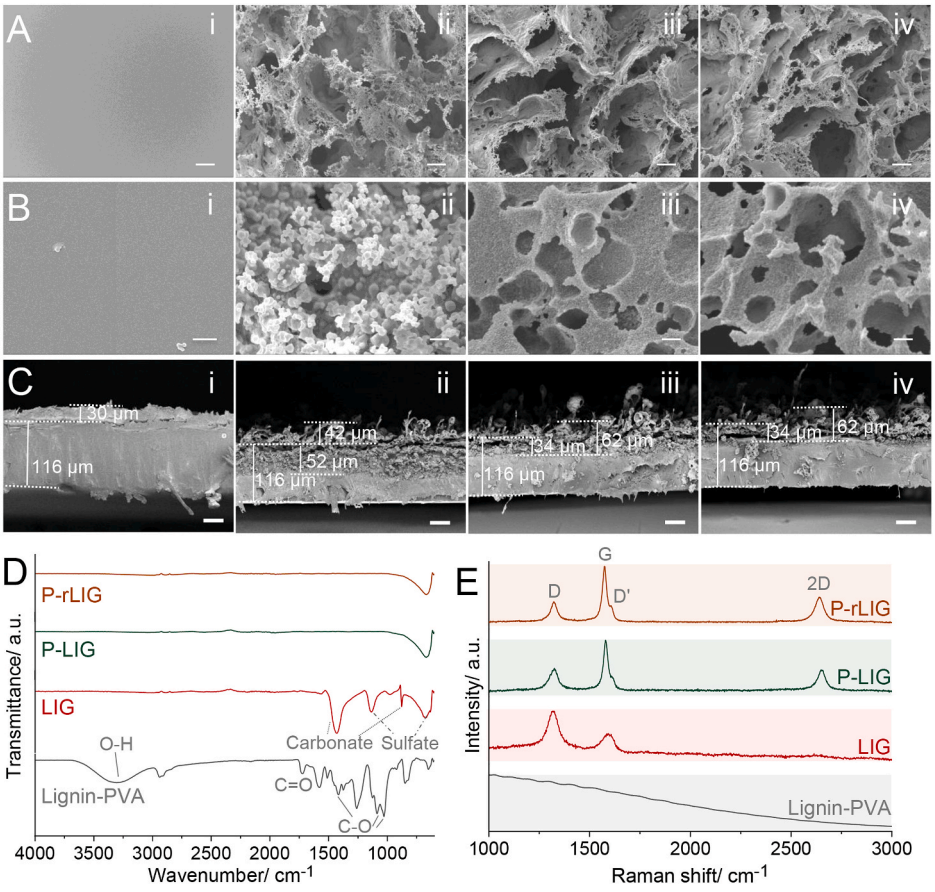


**Fig. 2.** Physicochemical properties. Top-view (A, low magnification with the scale bar of 20 μm; B, high magnification with the scale bar of 200 nm) and (C) cross-sectional SEM images (scale bar of 40 μm) of lignin-PVA (i), LIG (ii), P-LIG (iii) and P-rLIG (iv); (D) FTIR spectra and (E) Raman spectra.

fluorinated ethylene propylene (FEP) and polyether ether ketone (PEEK), the elastomer polydimethylsiloxane (PDMS), the thermosetting polyimide (PI) and to biomass cellulose derived paper (Fig. S5).

### 3.2. Physicochemical characterizations

The physicochemical properties of the optimized LIG derived from laser lithography and its further treatment with water lift-off (P-LIG) and $NaBH_4$ (P-rLIG) were examined with SEM, FTIR, Raman and XPS, respectively. Fig. 2A and B displays top-view SEM images of the pristine lignin-PVA film (i), LIG (ii), P-LIG (iii) and P-rLIG (iv) at two different magnifications, respectively. The lignin-PVA shows a compact and flat film on the PET substrate resulting from the blade-coating of the lignin dispersion with PVA as a polymeric binder. The thickness of the lignin-PVA layer on top of the PET is estimated to be ~30 μm according to the cross-sectional SEM image (Fig. 2C (i)). The laser irradiation converted the smooth lignin-PVA film into a coarse morphology with a hierarchical porous structure of the LIG in Fig. 2A (ii), while the high magnification SEM (Fig. 2B (ii)) reveals the appearance of granular particles attached to the LIG surface, which can be ascribed to the residues after the laser irradiation. These residues also appeared in the cross-sectional SEM image (Fig. 2C (ii)). For the P-LIG, the further water lift-off procedure contributed to the exposure of the deeper macro-pores for the P-LIG as shown in Fig. 2A (iii), as well as the removal of the granular residues attached to the LIG film with micro-pores (Fig. 2B (iii). The production of macro-/micro-pores in the P-LIG may be ascribed to not only the rapid release of gaseous products (e.g., $CO_2$, $H_2O$, $C_2H_2$) during the laser lithography process (Brannon et al., 1985; Srinivasan et al., 1987), but also to the dissolution of granular residues and un-reacted lignin-PVA by the water lift-off. The treatment of the P-LIG with $NaBH_4$ did not cause any obvious changes in the porous structure of graphene for the P-rLIG. The thickness of the graphene layer of the P-rLIG is around ~62 μm with a ~34 μm penetration into the PET layer (Fig. 2C (iii) and (iv)), which supports the retention/attachment of P-rLIG on the PET substrate. The EDS (Figs. S6 and S7) of the lignin-PVA shows a high oxygen content with an O/C ratio of 24.56%, and a low content of Na (1.6 at%) and S (0.34 at%). The O/C ratio value for the LIG decreased slightly to 22.00%, while the content of Na and S apparently increased to 4.28 and 0.88 at%, respectively. This can be ascribed to the accumulation of Na and S containing compounds as residues on the LIG. After the removal of these residues by water lift-off, the P-LIG displays a lower O/C ratio (3.24%) and lower Na (0.19 at%) and S (0.42 at%) content compared to that of the LIG. For the P-rLIG, the O/C ratio further decreased to 2.34% by the $NaBH_4$ reduction.

In the FTIR spectra in Fig. 2D, the lignin-PVA film shows several characteristic bands attributed to oxygen-containing functional groups (e.g., OH, C–O, C═O), which is consistent with pure lignin and PVA as listed in Fig. S8 and Table S1. Under laser irradiation, the above-mentioned oxygen-containing functional groups disappeared in the LIG due to the photothermal reaction, while several other strong and broad bands appeared in the spectrum. These new bands are assigned to carbonate and sulfate groups (Volz, 1983), indicating that the residues on the LIG surface (Fig. 2B (ii)) are inorganic compounds. It can be hypothesized that the laser irradiation locally provides a high energy that enables bond cleavage of the atoms (O, H, partially C) in lignin with released gaseous products and the re-organization of the aromatic ring into a graphene-like structure, while the Na and S accumulated in the resulting LIG in the form of Na-containing inorganic compounds (e.g., sodium sulfate and sodium carbonate). These inorganic compounds were removed by the water lift-off treatment, resulting in a relatively flat spectrum for the P-LIG and P-rLIG comparable to natural graphite powder (Fig. S8).

As shown in the Raman spectra in Fig. 2E, no obvious bands were noted for lignin-PVA except a lifted background signal in the low and medium vibrational frequency region (1000–2000 $cm^{-1}$) caused by laser induced fluorescence of lignin molecules (Prats-Mateu et al., 2018). Three main bands appeared for the LIG due to the laser induced graphitization, including a D band at 1319 $cm^{-1}$ related to the disordered structure of graphene, a G band at 1581 $cm^{-1}$ due to the $E_{2g}$ mode at the $\Gamma$-point arising from stretching of the sp2 C–C bond in graphitic materials with a week shoulder D′ band (1609 $cm^{-1}$) for randomly distributed impurities or surface charges, and a weak 2D band at 2623 $cm^{-1}$ for the stacking order of graphene layers (Nanda et al., 2016). Meanwhile, a slightly lifted background still exists for the LIG, which probably originates from the lignin residues on the LIG surface. For the P-LIG, the intensity of the G and 2D bands increases while the intensity of the D band decreases compared to that of the LIG. The intensity ratios of the D and 2D bands to the G band are widely employed as a sensitive metric for disorder degree and stacked graphene layers, respectively (Dresselhaus et al., 2010; Saito et al., 2011). The statistical analysis of $I_D/I_G$ and $I_{2D}/I_G$ ratios as well as the band position and fullwidth at half maximum (FWHM) are summarized in Table S2. The $I_D/I_G$ value decreases from 2.76 (LIG) to 0.75 (P-LIG), and the $I_{2D}/I_G$ ratio increases from 0.32 (LIG) to 0.76 (P-LIG), suggesting the exposure of a layered graphene structure after the removal of residues by water lift-off. The $NaBH_4$ reduction of the P-LIG contributed to a further decrease of the $I_D/I_G$ value to 0.56 and an increase of the $I_{2D}/I_G$ value to 0.88, which is consistent with the decreasing sheet resistance trend in the order LIG (34.3 Ω/sq), P-LIG (21.4 Ω/sq) and P-rLIG (17.1 Ω/sq).

The chemical characteristics of the LIG at different processing stages were further investigated by XPS with full survey spectra and high-resolution spectra of C1s, O1s and S2p. The XPS full survey (Fig. 3A) showed C1s (285 eV), O1s (532 eV) and Na1s (1070 eV) to be prevalent in lignin-PVA, LIG, P-LIG and P-rLIG. In addition, the band at 168 eV for LIG is attributed to S2p. It should be noted that S2p is not clearly visible in the full spectrum of lignin-PVA due to the insulating property of lignin-PVA and the low amount of S, but S2p could be detected via the high-resolution scan (Fig. 3D). Table 1 summarizes the atomic percentage of different elements. Compared to that of lignin-PVA, the LIG shows a decreased C/O ratio from 2.82 to 1.43, indicating an accumulation of oxygen on the surface of the LIG. This might be contributed by the sodium carbonate and sodium sulfate, which is consistent with the significantly increased Na (8.72%) and S (7.10%) compared to the lignin-PVA. The P-LIG possesses an increased C/O ratio to 7.16 with a trace amount of Na (0.49%) and no-detectable S after the water lift-off of the excess lignin-PVA and removal of inorganic compounds. These results are consistent with the SEM and FTIR results (Fig. 2), and validated

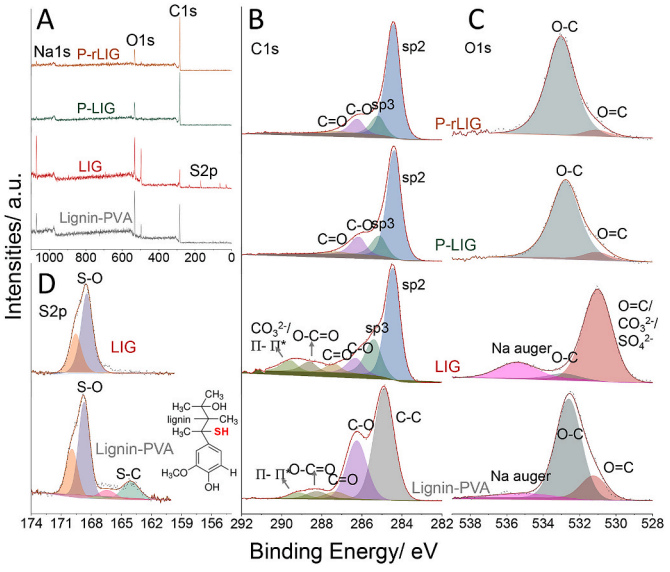


**Fig. 3.** XPS spectra. (A) full survey, (B) C1s, and (C) O1s of lignin-PVA, LIG, P-LIG and P-rLIG; (D) S2p of lignin-PVA and LIG, inset is the coniferyl alcohol unit of alkali lignin.

**Table 1**
XPS fitting results of the element composition and functional groups percentage for lignin-PVA, LIG, P-LIG and P-rLIG.

| Sample | Full survey/at% | | | | | C1s/% | | | | | O1s/% | |
|---|---|---|---|---|---|---|---|---|---|---|---|---|
| | C | O | Na | S | C/O | C–C/C═C | C–O | C═O | O–C═O | $CO_3^{2-}/\pi$-$\pi^*$ | O═C/$CO_3^{2-}$/$SO_4^{2-}$ | O–C |
| Lignin-PVA | 71.86 | 25.33 | 2.41 | 0.40 | 2.82 | 58.95 | 30.72 | 3.62 | 3.74 | 2.92 | 18.45 | 75.03 |
| LIG | 49.60 | 34.58 | 8.72 | 7.10 | 1.43 | 74.26 | 9.15 | 4.94 | 5.61 | 6.04 | 77.50 | 4.38 |
| P-LIG | 87.32 | 12.19 | 0.49 | – | 7.16 | 83.75 | 12.96 | 3.29 | – | – | 10.85 | 89.15 |
| P-rLIG | 90.12 | 9.36 | 0.52 | – | 9.63 | 88.14 | 9.77 | 2.09 | – | – | 7.50 | 92.50 |

the hypothesis proposed above. The $NaBH_4$ reduction promoted further removal of oxygen resulting in a higher C/O ratio value of 9.63.

Fig. 3B shows the high resolution C1s spectrum deconvoluted into different carbon-containing functional groups with detailed percentages listed in Table 1 (Collado et al., 2018; Cunge et al., 2015; Yang et al., 2020). The laser treatment of lignin-PVA cleavages the carbon-oxygen containing groups in the resulting LIG (down from 30.72% to 9.15%) with increased C–C/C═C as a result (up from 58.95% to 74.26%). The slightly increased intensity of C═O/O–C═O and the appearance of $CO_3^{2-}$ (Collado et al., 2018) for the LIG are indicative of the accumulation of inorganic compounds. A further increase of the C–C/C═C intensity and a decrease of the carbon-oxygen containing groups intensity for P-LIG and P-rLIG suggest an improved reduction degree. The high resolution O1s spectrum (Fig. 3C) shows that the O–C functional group dominates (>75%) for lignin-PVA, P-LIG and P-rLIG with a small amount of O═C (<20%), while the O–C accounts only for 4.38% in LIG and O═C/$CO_3^{2-}$/$SO_4^{2-}$ (77.50%) dominate instead (Rabchinskii et al., 2018). A conversion of S was revealed by the high resolution S2p spectra of lignin-PVA and LIG in Fig. 3D. For the lignin-PVA, the deconvolution of the main band at the low binding energy, i.e., $S2p_{3/2}$ and $S2p_{1/2}$ spin-orbit doublet, corresponds to the thiol group (R–SH) from the coniferyl alcohol unit of alkali lignin (Evdokimov et al., 2018). The main band at the high binding energy is due to the sulfate groups ($SO_4^{2-}$) originating from sulfate lignin in the kraft pulping process (Evdokimov et al., 2018). The laser treatment eliminated the thiol groups by the photothermal or photochemical breaking of C–S bonds and converted them into sulfate groups, forming sodium sulfate on the surface of the LIG.

### 3.3. Electrochemical kinetics

The LIG, P-LIG and P-rLIG electrodes were patterned into single freestanding working electrodes (Fig. 4A inset), and their electrochemical properties were investigated by CV and EIS. Fig. 4A shows the quasi-reversible redox peaks of the $Fe(CN)_6^{3-/4-}$ probe at the LIG, P-LIG and P-rLIG electrode surfaces with different peak current densities and peak-to-peak separations (ΔE). The voltammogram obtained from the LIG electrode exhibited an anodic peak current density of 82.1 ± 3.2 μA with a ΔE of 238 ± 7.6 mV. For the P-LIG electrode, the anodic peak current density showed a 1.23 time increase to 101.2 ± 4.9 μA compared to that of the LIG, and ΔE decreased to 178 ± 10.4 mV. The improved electrode kinetics of P-LIG can be attributed to not only the removal of insulating inorganic salts and excess lignin-PVA, but also to the exposure of deep macro-pores, which resulted in higher surface area. The anodic peak current density for the P-rLIG electrode is 117.3 ± 9.7 μA, which is 1.43 and 1.16 times higher than that of the LIG and the P-LIG electrodes. The P-rLIG electrode also possesses the lowest ΔE value of 160 ± 5 mV among all the LIG electrodes.

Fig. 4B shows the Nyquist plots of the EIS data for all three electrodes. All electrodes exhibit a semicircle feature in the high-frequency region related to the charge transfer resistance (Rct) and a straight-line feature in the low frequency region corresponding to the diffusion-controlled process. However, unlike the conventional Randles circuit for a simple "planar" electrode/electrolyte interface consisting of an active electrolyte resistance ($R_s$) in series with the parallel combination of a constant phase element (CPE) and an impedance of a faradaic

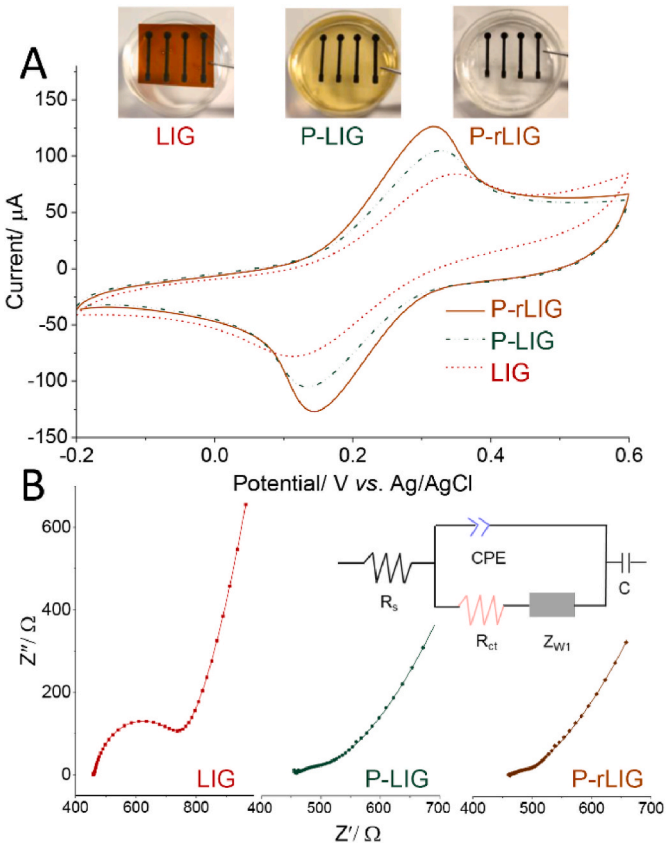


**Fig. 4.** Electrochemical kinetics measurements. (A) cyclic voltammograms of the LIG, P-LIG and P-rLIG electrodes (diameter 3 mm) in 5 mM $Fe(CN)_6^{3-/4-}$ in 0.1 M KCl, at a scan rate of 50 mV $s^{-1}$. The inset shows images of the LIG, P-LIG and P-rLIG electrodes; (B) EIS of the LIG, P-LIG and P-rLIG working electrode in 5 mM $Fe(CN)_6^{3-/4-}$ in 0.1 M KCl over the frequency range 0.01 Hz–100 kHz and at 5 mV amplitude. The inset shows the equivalent circuit fitting model.

reaction ($R_{ct}$) and a diffusion (Warburg, $Z_w$), the slope of the straight line in the low frequency region is higher than 1 (angle of 45°). Therefore, a double layer capacitance (C) is introduced in the equivalent circuit model (Fig. 4B inset) for the low frequency fitting. This might be related to mass transport in the porous electrodes. The detailed fitting parameters are summarized in Table S3. Compared to the LIG with a $R_{ct}$ value of 248.1 Ω, the P-LIG shows a significant increase in the electrode kinetics illustrated by the shrinking semicircle with a $R_{ct}$ value of 61.4 Ω. The P-rLIG electrode shows the lowest $R_{ct}$ value of 27.3 Ω, suggesting a faster electron-transfer rate at the electrode surface due to a higher reduction degree with improved conductivity, which is consistent with the results from the CV and the 4-point probe measurements. Thus, the P-rLIG electrode was used as the disposable electrode platform for the development of an electrochemical lactate biosensor.

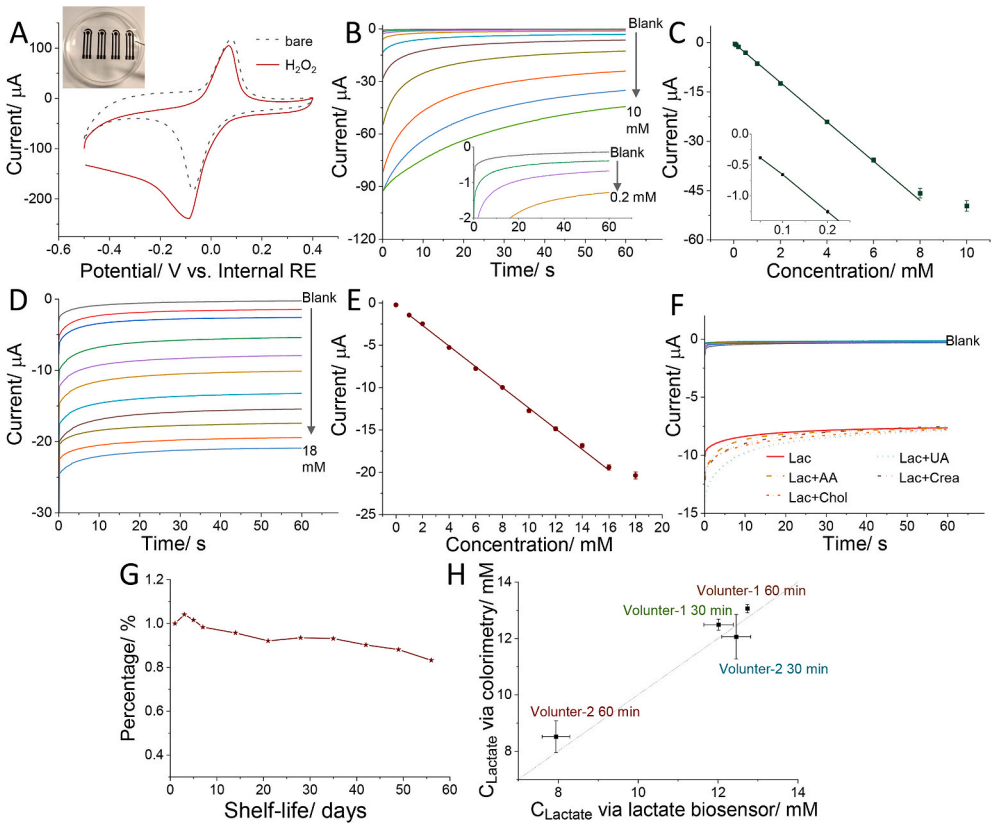


**Fig. 5.** Electrochemical lactate biosensors. (A) Cyclic voltammograms of PB/P-rLIG electrode in 5 mM $H_2O_2$ in 0.1 M PBS (pH = 6.4), scan rate of 50 mV $s^{-1}$; (B) amperometric response of PB/P-rLIG electrode to $H_2O_2$ from blank up to 10 mM in 0.1 M PBS (pH = 6.4) at −0.15 V vs internal RE, inset is an enlarged plot to 0.2 mM; (C) corresponding calibration curve of PB/P-rLIG electrode to $H_2O_2$, n = 3, inset is an enlarged plot in the range to 0.2 mM; (D) amperometric response of LOx/PB/P-rLIG electrode to lactate from blank up to 18 mM in artificial sweat (pH = 6.5) at −0.15 V vs internal RE; (E) corresponding calibration curve of LOx/PB/P-rLIG electrode to lactate, n = 3; (F) interference study of 0.01 mM ascorbic acid (AA), 0.059 mM uric acid (UA), 0.084 mM creatinine (Crea) and 1.2 mM cholesterol (Chol) in the appearance of 6 mM lactate; (G) shelf-life study of the integrated LOx/P-rLIG electrode towards 6 mM lactate in artificial sweat (pH = 6.5) at −0.15 V vs internal RE; (H) correlation of the LOx/P-rLIG biosensor with a standard colorimetric assay for real sweat sample analysis.

### *3.4. Disposable lignin-derived electrodes for electrochemical lactate biosensors*

A three-electrode system based on the P-rLIG (Fig. 5A inset) was developed of the disposable electrode for electrochemical lactate biosensors, consisting of a working electrode, a counter electrode and an internal reference electrode coated with Ag/AgCl ink. Porous P-rLIG provides an excellent heterostructured platform for the functionalization with PB and successive immobilization with enzyme. The P-rLIG electrode serves as an electrochemical transducer for the reduction of $H_2O_2$ which is a common intermediate originating from the enzymatic catalytic reaction of biomarkers via various oxidases (e.g., lactate oxidase and glucose oxidase). Fig. 5A exhibits the CV response of the PB/P-rLIG electrode towards 5 mM $H_2O_2$ in 0.1 M PBS (pH = 6.4) with the reduction peak current increasing from 181.0 μA (without $H_2O_2$) to 240.1 μA resulting from the reduction reaction of PB towards $H_2O_2$. The amperometric response (Fig. 5B) of the PB/P-rLIG electrode increased gradually with increasing $H_2O_2$ over the dynamic range up to 10 mM at −0.15 V (optimized applied potential). The corresponding calibration curve (Fig. 5C) was linear for $H_2O_2$ concentrations up to 8 mM ($R^2$ = 0.999) with a sensitivity of 5.98 μA $mM^{-1}$. The limit of detection (LOD) was calculated to be 7 μM based on $3S_B/S$ ($S_B$ is the standard deviation of 10 measurements in blank, S is the sensitivity) according to the IUPAC recommendation (da Silva and Machado, 2012).

Based on the good analytical performance of the PB/P-rLIG electrode response to $H_2O_2$, LOx was immobilized onto the electrode by chitosan to create disposable electrochemical biosensors for lactate detection (LOx/PB/P-rLIG) with an extra porous polycarbonate membrane for encapsulation and as a diffusion layer for wide linear range. The performance of the disposable lactate biosensor in response to lactate in artificial sweat (pH = 6.5) was then investigated and the amperometric response is shown in Fig. 5D. The amperometric curves exhibit a well-defined current response to the dynamic concentration range of lactate up to 18 mM with a fast response time reaching a stable current value within 20 s. According to the calibration curve in Fig. 5E, the current response of the electrode was linearly proportional to lactate concentration up to 16 mM ($R^2$ = 0.997), with a high sensitivity of 1.21 μA $mM^{-1}$ (i.e., 17.1 μA $mM^{-1}$ $cm^{-2}$). The LOD was calculated to be 0.20 mM. The sensitivity of the fabricated LOx/PB/P-rLIG electrode towards lactate biosensing is comparable to, and in some cases higher than, reported values of other carbon-based disposable electrodes for lactate biosensors in the literature, such as a PB/screen-printed graphite electrode (0.553 μA $mM^{-1}$) (Kim et al., 2014), a tetrathiafulvalene/screen-printed carbon fiber-based electrode (0.644 μA $mM^{-1}$) (Jia et al., 2013), a Pt-carbon nanofiber/screen-printed carbon electrode (36.8 μA $mM^{-1}$ $cm^{-2}$) (Lamas-Ardisana et al., 2014), a Pt/laser-scribed graphitic carbon (35.8 μA $mM^{-1}$ $cm^{-2}$) (Madden et al., 2022) and a MCNTs-Os/graphite-based electrode (0.74 μA $mM^{-1}$) (Zhang et al., 2020). The good analytical performance is likely facilitated by the porous structure with high surface area and improved electrochemical kinetics resulting from the laser lithography, water lift-off and $NaBH_4$ treatment. This approach makes good use of a waste material, *i.e.*, lignin, for its conversion into graphene electrodes, that are comparable to reported carbon-based electrodes regarding the analytical performance.

To evaluate the selectivity of the disposable lactate biosensors, the response toward 6 mM lactate in artificial sweat (pH = 6.5) was tested in the presence of potential interferences in their physiological concentrations commonly used in perspiration and dermal analysis (Kim et al., 2014; Payne et al., 2019), including 0.01 mM AA, 0.059 mM UA, 0.084 mM creatinine and 1.2 mM cholesterol. As shown in Fig. 5F, these interferences have a negligible effect on the detection of lactate, indicating a good selectivity of the fabricated lactate biosensors. The reproducibility of the disposable lactate biosensing electrodes was evaluated by the measurement of 6 mM lactate in artificial sweat with seven electrodes. The relative standard deviation (RSD) value was calculated to be 6.89%. The shelf-life of the disposable lactate biosensors was tested by keeping the electrodes in a sealed container inside a refrigerator (4 °C)

over a period of eight weeks and regularly measuring the signal response to 6 mM of lactate with a fresh electrode. The electrodes showed an excellent shelf-life (Fig. 5G) in the first two weeks with a ±5% deviation of the response to the initial response value (first day measurement). The response remained within 90% of the initial response value over six weeks, while it dropped to around 83% of the initial response value after eight weeks, indicating a good shelf-life of the fabricated disposable lactate biosensors kept at 4 °C.

To validate the feasibility for real sample analysis, the developed lactate biosensors were applied for the determination of lactate levels in real sweat samples collected from two healthy volunteers after 30- and 60-min running exercises. Well-defined steady state responses were observed for the four human sweat samples with a 3-fold dilution in artificial sweat (Fig. S9). As shown in Fig. 5H, the measured lactate levels from the biosensors showed a very good correlation (i.e., all data points approaching the line with a slope of 1) with the colorimetric assay, suggesting the potential application for point-of-care detection of lactate levels during physical exercise.

## 4. Conclusion

In summary, we have demonstrated a green route for lignin-derived graphene electrodes, serving as a disposable electrode for electrochemical biosensors with good performance. Lignin is often discarded as a by-product and waste in the paper industry, overlooking its value as an aromatic ring-rich and sustainable carbon precursor that could be patterned and converted into a conductive graphene film via an energy-saving localized photothermal process. Surface and spectroscopic characterization results revealed the formation of LIG induced by the photothermal process and a new observation on the formation of inorganic compounds during the laser lithography. The inorganic residues and the unreacted lignin can simply be removed by water lift-off, to produce patterned lignin-derived graphene. $NaBH_4$ treatment further increased the conductivity of the P-rLIG resulting in enhanced electrochemical kinetics. The porous P-rLIG serves as a 3D matrix for the fabrication of disposable electrochemical lactate biosensors with good analytical performance (wide linear range, high sensitivity, and long shelf-life time). This technique can broaden the spectrum of lignin utilization strategies, taking into consideration its low cost, bio-renewability, and abundance in nature, for the realization of a sustainable society. The resulting P-rLIG could serve as a general disposable platform for development of various single or multiplexed sensors and biosensors via functionalization or by immobilization of biorecognition elements. Beyond this, the technique is versatile for different flexible substrates including thermoplastics, elastomers, thermosets, and biomass and other biodegradable substrates, which is promising for the development of fully sustainable and biodegradable biosensors. Furthermore, the combination of this technique for the fabrication of a disposable electrode platform with other automated coating techniques (e.g., ink-jet printing, spray coating, screen printing etc.) for functional material and biorecognition element modification could be beneficial for high-throughput production of the final biosensing devices.

## CRediT authorship contribution statement

**Lingyin Meng:** Conceptualization, Methodology, Formal analysis, Investigation, Writing – original draft, Writing – review & editing, Supervision. **Sorana Chirtes:** Investigation, and Formal analysis (LIG and electrochemistry). **Xianjie Liu:** Investigation, and, Formal analysis, (XPS). **Mats Eriksson:** Formal analysis, Investigation, Writing – review & editing. **Wing Cheung Mak:** Conceptualization, Methodology, Formal analysis, Investigation, Writing – review & editing, Supervision.

## Declarationof competing interest

The authors declare that they have no known competing financial interests or personal relationships that could have appeared to influence the work reported in this paper.

## Data availability

Data will be made available on request.

## Acknowledgments

The authors would like to acknowledge the Swedish Research Council (VR-2015-04434) for generous financial support to carry out this research.

## Appendix A. Supplementary data

Supplementary data to this article can be found online at https://doi.org/10.1016/j.bios.2022.114742.

## Supplementary data

.

## References

Ahmed, M.U., Hossain, M.M., Safavieh, M., Wong, Y.L., Rahman, I.A., Zourob, M., Tamiya, E., 2016. Crit. Rev. Biotechnol. 36 (3), 495–505.
Bettazzi, F., Marrazza, G., Minunni, M., Palchetti, I., Scarano, S., 2017. Compr. Anal. Chem. 77, 1–33.
Brannon, J.H., Lankard, J., Baise, A., Burns, F., Kaufman, J., 1985. J. Appl. Phys. 58 (5), 2036–2043.
Collado, L., Reynal, A., Fresno, F., Barawi, M., Escudero, C., Perez-Dieste, V., Coronado, J.M., Serrano, D.P., Durrant, J.R., de la Peña, O.S., 2018. Nat. Commun. 9 (1), 1–10.
Cunge, G., Ferrah, D., Petit-Etienne, C., Davydova, A., Okuno, H., Kalita, D., Bouchiat, V., Renault, O., 2015. J. Appl. Phys. 118 (12), 123302.
da Silva, O.B., Machado, S.A., 2012. Anal. Methods 4 (8), 2348–2354.
Dresselhaus, M.S., Jorio, A., Hofmann, M., Dresselhaus, G., Saito, R., 2010. Nano Lett. 10 (3), 751–758.
Edberg, J., Brooke, R., Hosseinaei, O., Fall, A., Wijeratne, K., Sandberg, M., 2020. npj Flex. Electron. 4 (1), 1–10.
El-Kady, M.F., Kaner, R.B., 2013. Nat. Commun. 4, 1475.
El-Kady, M.F., Strong, V., Dubin, S., Kaner, R.B., 2012. Science 335 (6074), 1326–1330.
Evdokimov, A.N., Kurzin, A.V., Fedorova, O.V., Lukanin, P.V., Kazakov, V.G., Trifonova, A.D., 2018. Wood Sci. Technol. 52 (4), 1165–1174.
Fang, W., Yang, S., Wang, X.-L., Yuan, T.-Q., Sun, R.-C., 2017. Green Chem. 19 (8), 1794–1827.
Fenzl, C., Nayak, P., Hirsch, T., Wolfbeis, O.S., Alshareef, H.N., Baeumner, A.J., 2017. ACS Sens. 2 (5), 616–620.
Htwe, Y., Abdullah, M., Mariatti, M., 2021. Synth. Met. 274, 116719.
Jia, W., Bandodkar, A.J., Valdés-Ramírez, G., Windmiller, J.R., Yang, Z., Ramírez, J., Chan, G., Wang, J., 2013. Anal. Chem. 85 (14), 6553–6560.
Kim, J., Valdés-Ramírez, G., Bandodkar, A.J., Jia, W., Martinez, A.G., Ramírez, J., Mercier, P., Wang, J., 2014. Analyst 139 (7), 1632–1636.
Lamas-Ardisana, P.J., Loaiza, O.A., Añorga, L., Jubete, E., Borghei, M., Ruiz, V., Ochoteco, E., Cabañero, G., Grande, H.J., 2014. Biosens. Bioelectron. 56, 345–351.
Lee, H., Lim, C.H.J., Low, M.J., Tham, N., Murukeshan, V.M., Kim, Y.-J., 2017. Int. J. Precis. Eng. Manuf. 4 (3), 307–322.
Li, G., 2020. J. Appl. Phys. 127 (1), 010901.
Lin, J., Peng, Z., Liu, Y., Ruiz-Zepeda, F., Ye, R., Samuel, E.L., Yacaman, M.J., Yakobson, B.I., Tour, J.M., 2014. Nat. Commun. 5 (1), 1–8.
Ma, Q., Yu, Y., Sindoro, M., Fane, A.G., Wang, R., Zhang, H., 2017. Adv. Mater. 29 (13), 1605361.
Madden, J., Vaughan, E., Thompson, M., O'Riordan, A., Galvin, P., Iacopino, D., Teixeira, S.R., 2022. Talanta 246, 123492.
Mahdi, M.A., Yousefi, S.R., Jasim, L.S., Salavati-Niasari, M., 2022. Int. J. Hydrogen Energy 47 (31), 14319–14330.
Meng, L., Turner, A.P., Mak, W.C., 2020. Biotechnol. Adv. 39, 107398.
Meng, L., Turner, A.P.F., Mak, W.C., 2021. ACS Appl. Mater. Inter. 13 (45), 54456–54465.
Mohamed, H.M., 2016. TrAC, Trends Anal. Chem. 82, 1–11.
Moro, G., Bottari, F., Van Loon, J., Du Bois, E., De Wael, K., Moretto, L.M., 2019. Biosens. Bioelectron. 146, 111758.
Nanda, S.S., Kim, M.J., Yeom, K.S., An, S.S.A., Ju, H., Yi, D.K., 2016. TrAC, Trends Anal. Chem. 80, 125–131.
Newman, J.D., Turner, A.P., 2005. Biosens. Bioelectron. 20 (12), 2435–2453.
Pani, D., Achilli, A., Bonfiglio, A., 2018. Adv. Mater. Technol. 3 (10), 1800008.
Payne, M.E., Zamarayeva, A., Pister, V.I., Yamamoto, N.A., Arias, A.C., 2019. Sci. Rep. 9 (1), 1–10.
Pistone, A., Espro, C., 2020. Curr. Opin. Green Sustain. Chem. 26, 100374.

Pradhan, S., Brooks, A., Yadavalli, V., 2020. Mater. Today Bio 7, 100065.
Prats-Mateu, B., Bock, P., Schroffenegger, M., Toca-Herrera, J.L., Gierlinger, N., 2018. Sci. Rep. 8 (1), 1–12.
Rabchinskii, M.K., Dideikin, A.T., Kirilenko, D.A., Baidakova, M.V., Shnitov, V.V., Roth, F., Konyakhin, S.V., Besedina, N.A., Pavlov, S.I., Kuricyn, R.A., 2018. Sci. Rep. 8 (1), 1–11.
Saito, R., Hofmann, M., Dresselhaus, G., Jorio, A., Dresselhaus, M., 2011. Adv. Phys. 60 (3), 413–550.
Srinivasan, R., Braren, B., Dreyfus, R., 1987. J. Appl. Phys. 61 (1), 372–376.
Srinivasan, R., Hall, R., Wilson, W., Loehle, W., Allbee, D., 1994. Synth. Met. 66 (3), 301–307.
Turner, A.P., 2013. Chem. Soc. Rev. 42 (8), 3184–3196.
Volz, F.E., 1983. Appl. Opt. 22 (12), 1842–1855.
Wang, J., Nie, P., Ding, B., Dong, S., Hao, X., Dou, H., Zhang, X., 2017. J. Mater. Chem. 5 (6), 2411–2428.
Xiong, Z., Guo, P., Yuan, S., Sun, S., Wang, C., Gao, Y., 2021. Energy Fuels 35 (20), 16903–16914.
Xu, M., Obodo, D., Yadavalli, V.K., 2019. Biosens. Bioelectron. 124, 96–114.
Yan, J., Rodrigues, M.T.F., Song, Z., Li, H., Xu, H., Liu, H., Wu, J., Xu, Y., Song, Y., Liu, Y., 2017. Adv. Funct. Mater. 27 (22), 1700653.
Yáñez-Sedeño, P., Campuzano, S., Pingarrón, J.M., 2020. Biosensors 10 (7), 76.
Yang, Z., Gleisner, R., H Mann, D., Xu, J., Jiang, J., Zhu, J., 2020. Polymers 12 (12), 2829.
Ye, R., Chyan, Y., Zhang, J., Li, Y., Han, X., Kittrell, C., Tour, J.M., 2017. Adv. Mater. 29 (37), 1702211.
Yousefi, S.R., Masjedi-Arani, M., Morassaei, M.S., Salavati-Niasari, M., Moayedi, H., 2019. Int. J. Hydrogen Energy 44 (43), 24005–24016.
Yousefi, S.R., Sobhani, A., Alshamsi, H.A., Salavati-Niasari, M., 2021. RSC Adv. 11 (19), 11500–11512.
Zhang, L., Liu, J., Fu, Z., Qi, L., 2020. J. Nanosci. Nanotechnol. 20 (3), 1495–1503.
Zhang, W., Lei, Y., Ming, F., Jiang, Q., Costa, P.M.F.J., Alshareef, H.N., 2018. Adv. Energy Mater. 8 (27).
Zhang, W., Yin, J., Wang, C., Zhao, L., Jian, W., Lu, K., Lin, H., Qiu, X., Alshareef, H.N., 2021. Small Methods 5 (11), 2100896.
Zhao, D., Zhu, Y., Cheng, W., Chen, W., Wu, Y., Yu, H., 2021. Adv. Mater. 33 (28), 2000619.
Zhu, J., Yan, C., Zhang, X., Yang, C., Jiang, M., Zhang, X., 2020. Prog. Energy Combust. Sci. 76, 100788.